

Interferometric validation of image based wavefront sensing for NGST

Joseph J. Green, David C. Redding, Yuri Beregovski, Andrew E. Lowman
and Catherine M. Ohara

Jet Propulsion Laboratory; 4800 Oak Grove Dr., Pasadena, CA 91109

ABSTRACT

To achieve and maintain excellent imaging performance, the Next Generation Space Telescope (NGST) will employ image based phase retrieval methods to control its segmented primary mirror. In this paper, we present the experimental validation of a focus-diverse wavefront sensing (WFS) algorithm with comparative interferometric measurements of a perturbed test mirror. Using sets of defocused point-spread functions measured with the NGST phase retrieval camera, we estimate the wavefront of the test optic in a perturbed and unperturbed state. Interleaved with the focus-diverse sets, we measure the surface figure of the mirror using a ZYGO interferometer. After reviewing the basic WFS algorithm and describing the experimental setup, we show that we can obtain agreement that is better than 1/100th of a wave rms in the difference of the wavefront estimates obtained in the perturbed and unperturbed states. Essentially, this work demonstrates that our image based WFS methods are generally competitive with standard industrial optical metrology instruments.

Keywords: NGST, phase retrieval, focus diversity, wavefront sensing, interferometry

1. INTRODUCTION

The Next Generation Space Telescope (NGST) will possess an actively controlled, segmented primary mirror (PM) as part of its optical telescope assembly (OTA). The PM requires active control to reduce its structural stability requirements as well as to mitigate the many risks associated with having a static observatory. With the proper sensing and control of PM and secondary mirror misalignments and figure errors, NGST will be able to maintain the strict optical performance specifications outlined in the high level observatory requirements.

The initial fine phasing and subsequent maintenance of the observatory will be conducted through use of the Modified Gerchberg-Saxton (MGS) WFS algorithm [1]. This image-based algorithm processes a pupil image along with a diverse set of defocused point-spread function (PSF) measurements into an estimate of the exit-pupil phase aberrations. Because these measurements are taken at a science focal plane, the estimated aberrations can be made without the use of a large number of non-common path optics that require accurate calibration. The MGS algorithm has been implemented and extensively tested on NGST Government testbeds. Through many experiments, this method has proven effective in the calibration and use of deformable mirrors and mirror segment actuators to control wave front error, [2]. Refer to [1] for a more complete discussion of this method.

In a typical wavefront control (WFC) experiment a set of actuator controls are derived from an estimated wavefront error (WFE) function. Subsequent wavefront estimations reveal the residual, post-control WFE. While its convenient to use the WFS estimates themselves to gauge the system performance, there is the risk that an unobservable bias may exist somewhere within this process. To a level, we overcome this risk by making careful data consistency checks. This is done by comparing the PSF measurements to PSF models computed from exit-pupil phase estimates. Although we have never encountered such biases, this data consistence check would signal the existence significant biases in the recovered optical path difference (OPD) map. While this data consistency check validates the WFS process, it does so at the *focal plane* in way that is not truly independent of the optical system itself. Furthermore, it is difficult to numerically evaluate the data consistency errors in a way that helps model the actual WFS errors.

To achieve an independent and rigorous validation of the MGS WFS algorithm at the *pupil plane*, we employ a commercial interferometer. Specifically, we use a ZYGO GPI interferometer to provide independent metrology of a test optic for direct comparison with the estimates that we obtained with the NGST phase retrieval camera (PRC). The PRC encapsulates our image-based methodology in portable platform that has a similar form factor to commercial metrology equipment, [3]. By directly comparing the recovered OPD maps observed over the course of the experiment, we can establish a very high level of validation for the baseline NGST WFS algorithm

2. ARRANGEMENTS FOR COMPARATIVE OPTICAL METROLOGY

2.1 The test optic

As a basis for conducting our comparative metrology experiment, we use a reflective test optic with fiducial markings. The mirror is a 2-inch sphere with a 200mm radius of curvature. It is mounted with a non-symmetric structured mask, as shown in figure 1. The mask provides features that allow for accurate scaling and co-registration of the ZYGO and PRC OPD measurements.

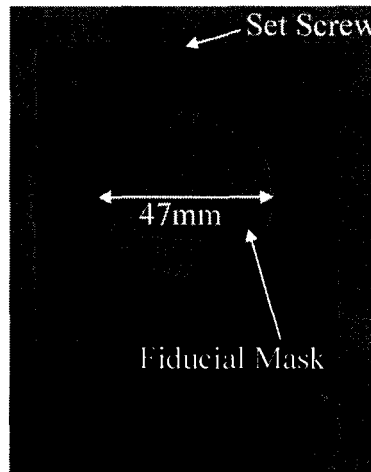


Figure 1: The test optic is mounted with a fiducial mask.

2.2 Optical metrology setups

Figures 2 and 3 show schematics for the respective ZYGO and PRC optical setups. Unfortunately, these setups do not allow for the simultaneous measurement of the test optic. To obtain measurements from both instruments, the mounted test optic has to be moved and realigned.

When the measurements were made with the ZYGO interferometer, a F/3.3 transmission sphere was used to null the nominal figure of the test optic. Although this instrument possesses a high measurement accuracy and repeatability, the laboratory conditions and the quality of the transmission sphere place limits on its performance in practice. During the course of the experiment, we took repeated measurements to reduce the impact of lab seeing, table vibrations and alignment repeatability errors.

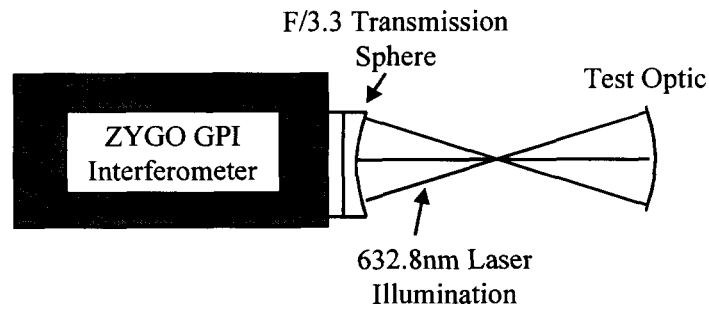


Figure 2: Schematic of the ZYGO measuring the test optic.

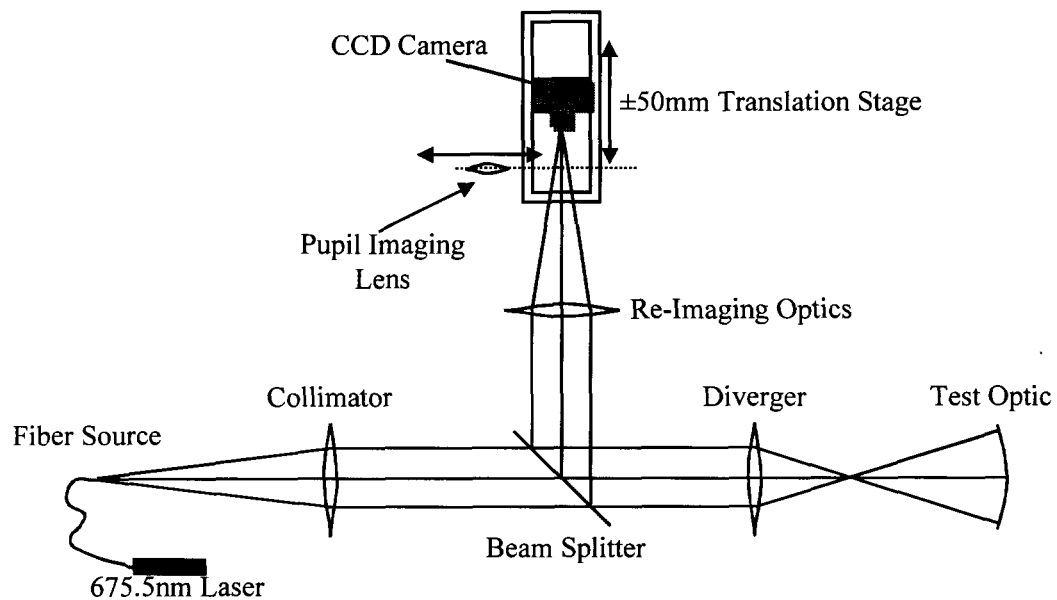


Figure 3: Schematic of the PRC measuring the test optic

Just as in the ZYGO interferometer, the nominal PRC configuration launches a collimated beam. To test a powered optic, an appropriate diverger lens must be selected to match the test optic curvature. This configuration of the PRC places the test optic at pupil location in the system and brings the reflected light to a focus at the camera. The camera is on a translations stage so that various levels of defocus can be induced over an ensemble of images to provide a focus-diverse set of measurements. Additionally, the PRC has a flip-in pupil imaging lens that allows for measurements of the exit-pupil intensity. Refer to [3] for a more detailed description of the PRC optical design and operation.

Using an image of the pupil and a diverse set of defocused PSF images, the MGS algorithm estimates the exit-pupil phase function. Figure 4 depicts an example of the required MGS data and the resulting OPD estimate. The levels of defocus depicted in figure 4 are representative of the PRC data taken throughout this experiment.

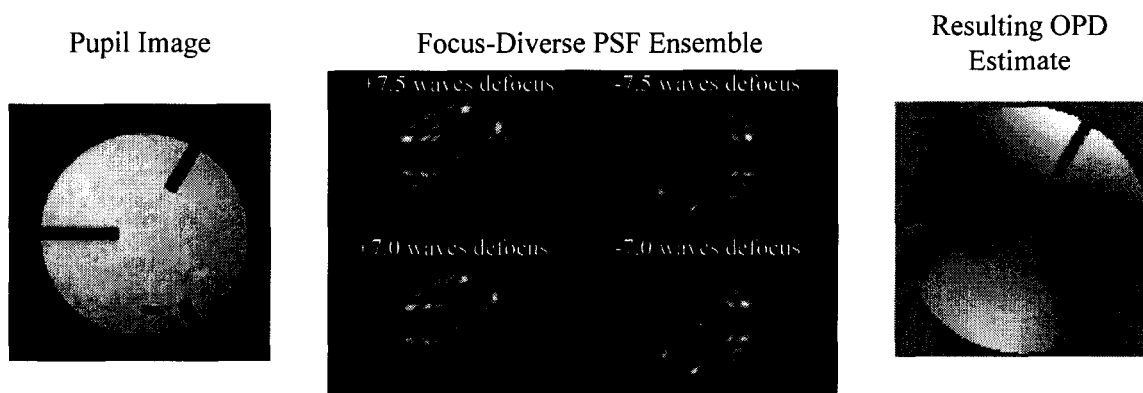


Figure 4: Example of a pupil image, focus-diverse PSF images and the resulting MGS OPD estimate.

3. EXPERIMENTAL PROCEDURE AND RESULTS

3.1 Procedure

Both the ZYGO and the PRC have imperfect optics whose aberrations bias the metrology of the test optic. To calibrate away these biases we could use a reference sphere but this would complicate the analysis and introduce yet another bias (i.e. the reference optic aberrations). Instead of using an independent reference, we take comparative measurements of the test optic in two difference states. Thus, the actual comparison of the instrument estimates is not made on the individual OPD maps but rather on the OPD map differences.

The initial state of the optic is simply what it is in its nominally mounted condition. After repeated measurements of the test optic are taken with the PRC and ZYGO, the mount setscrew is tightened to induce aberrations. The newly deformed mirror is then left alone for a period of time to allow the surface figure to stabilize. Then repeated sets of measurements are taken again with the two instruments. Table 1 documents the complete sequence of measurements along with the respective timing of the sequences.

Table 1: Sequence of measurement taken of the test optic over the course of the experiment

| Measurement Sequence | Elapsed Time (days:hours:minutes) | Measurement Description / Event | Number of Measurements | Sequence Label |
|----------------------|-----------------------------------|--|------------------------|--------------------|
| | 00:00:00 | Mirror placed in its mount | | |
| 1 | 02:17:10 | Mirror in initial state aligned to PRC | 3 | PRC _{1a} |
| 2 | 02:18:04 | Mirror in initial state aligned to ZYGO | 5 | ZYGO _{1a} |
| 3 | 02:18:32 | Mirror in initial state realigned to PRC | 2 | PRC _{1b} |
| 4 | 02:18:49 | Mirror in initial state realigned to ZYGO | 5 | ZYGO _{1b} |
| | 02:19:00 | Setscrew tightened to induce aberrations | | |
| 5 | 10:21:30 | Mirror in deformed state realigned to ZYGO | 3 | ZYGO _{2a} |
| 6 | 10:21:56 | Mirror in deformed state aligned to PRC | 2 | PRC _{2a} |
| 7 | 10:22:22 | Mirror in deformed state realigned to ZYGO | 5 | ZYGO _{2b} |
| 8 | 10:22:48 | Mirror in deformed state realigned to PRC | 10 | PRC _{2b} |

3.2 Experimental results and repeatability

The repeated measurements in each sequence help to reduce the zero-mean errors that occur due to noise processes and laboratory seeing. Through each stack of measurements we compute the mean OPD and its standard deviation. Figure 5 provides an example of the OPD maps we estimate from measurement sequences. Here we show the mean and standard deviation for the OPD estimates in the sequences labeled PRC_{2b} and $ZYGO_{2b}$ in table 1.

As expected, there are significant differences in mean OPD maps estimated by the PRC and ZYGO. The internal aberrations within each instrument induce superfluous phase aberrations that mix in with the apparent test optic errors. Looking at the standard deviations of the OPD maps, we find additional differences. The standard deviation images represent the temporal variations per OPD element over the sequence ensemble. Unlike the PRC, the deviations in the ZYGO measurement appear to be spatially correlated. This is most likely due to laboratory seeing. Although the PRC variations seem less correlated, the variations are generally higher at the edges than near the center and for both instruments the average deviation comes out to about 2.4nm per OPD element.

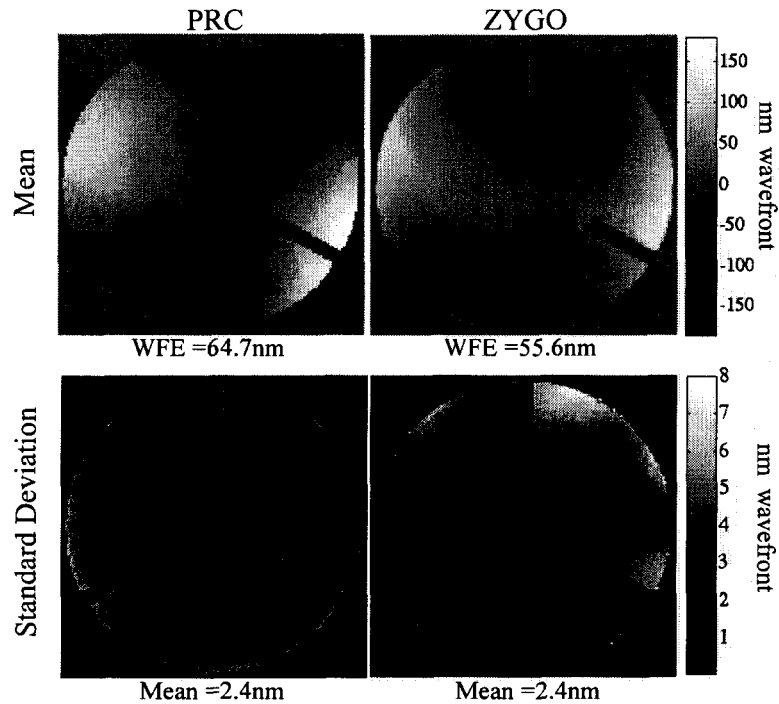


Figure 5: PRC and ZYGO OPD results from sequence PRC_{2b} and $ZYGO_{2b}$.

In both PRC and ZYGO estimates, the WFS performance at the pupil edges appears to be less repeatable than in the interior of pupil. This is not surprising because the edges of a pupil function are ill defined for any fixed choice of sampling. For the sake of making more meaningful comparisons, we mask off the entire perimeters of the OPD estimates by one element. In terms of area, this reduces the clear pupil region by about four percent. All values for shown for WFE and standard deviation are computed strictly within this reduced clear pupil region.

Table 2 shows the ensemble of results from all the sequences in the experiment. Listed in this table are the root-mean square (RMS) levels of the sequence-mean OPD maps and the average deviation per OPD element. With the assumption that the variations follow zero-mean Gaussian statistics, we also compute the net uncertainty as the ensemble deviation divided by the square root of the number of estimates.

Table 2: Summary of the sequence-averaged results.

| Average of Sequence | RMS WFE of Average OPD (nm) | Average Deviation Per Element in OPD (nm) | Uncertainty Per Element in OPD Average (nm) |
|---------------------|-----------------------------|---|---|
| PRC _{1a} | 33.93 | 2.21 | 1.28 |
| PRC _{1b} | 35.15 | 2.18 | 1.54 |
| PRC _{2a} | 65.79 | 1.49 | 1.06 |
| PRC _{2b} | 64.71 | 2.39 | 0.76 |
| ZYGO _{1a} | 17.66 | 3.89 | 1.74 |
| ZYGO _{1b} | 16.10 | 2.71 | 1.21 |
| ZYGO _{2a} | 56.83 | 1.42 | 0.82 |
| ZYGO _{2b} | 55.58 | 2.40 | 1.08 |

To reduce the experimental error caused by the repeatability of aligning the test-optic to an instrument, we acquire multiple data sequences with a given mirror state with each instrument. By computing the average OPD map over these two sessions we obtain estimates with significantly reduced uncertainties. The PRC and ZYGO OPD maps computed from their respective combined sequences are shown in figure 6 and 7 below. Table 3 lists the RMS WFE and the residual uncertainty for the combined estimates.

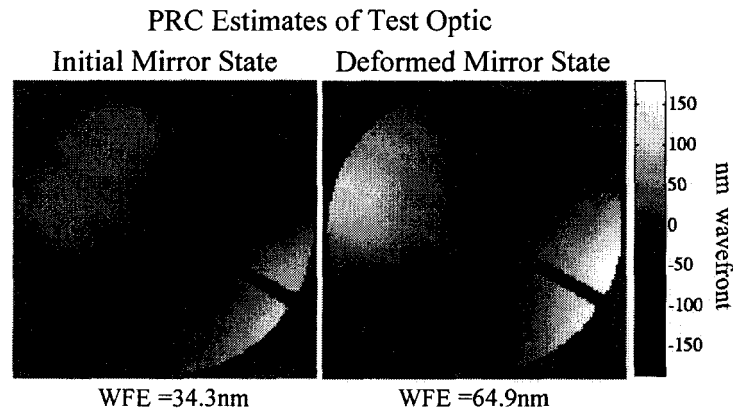


Figure 6: Combined PRC OPD estimates of the test-optic in it initial state (left) and deformed state (right).

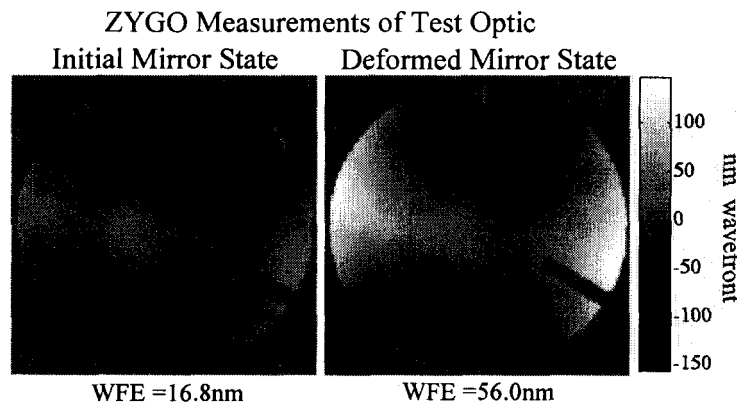


Figure 7: Combined ZYGO OPD estimates of the test-optic in it initial state (left) and deformed state (right).

Table 3: RMS WFE and net uncertainty of the combined OPD estimates

| Combined Measurements | Total Number of Estimates Combined | RMS WFE of Average OPD (nm) | Uncertainty Per Element in OPD Average (nm) |
|-----------------------|------------------------------------|-----------------------------|---|
| PRC ₁ | 5 | 34.33 | 1.42 |
| PRC ₂ | 12 | 64.87 | 0.79 |
| ZYGO ₁ | 10 | 16.77 | 1.22 |
| ZYGO ₂ | 8 | 56.02 | 1.00 |

4. VALIDATION OF THE MGS WFS ALGORITHM

We now have good estimates of the test optic for the two states of aberration as observed by each instrument. As mentioned earlier, the PRC and ZYGO have internal aberrations that induce biases into their respective estimates of the test optic. We can calibrate out the internal aberrations of each instrument by computing the difference of the test optic OPD maps in the two states. The difference of the OPD maps represents a scaled version of the setscrew influence function. By basing the comparison of the two WFS methodologies on the influence functions, we eliminate any static biases that are induced by the instruments.

The setscrew influence function is computed as the difference of the deformed state and the initial state. Figure 8 shows the PRC and ZYGO based estimates of this influence function along with the difference. Table 4 lists the RMS of the influence function and the net uncertainty of its computation. As shown below, the difference of the PRC and ZYGO influence function estimates is only $3.8nm$ RMS with a $\pm 2.3nm$ uncertainty. Thus, we conclude from this result that the performance of NGST WFS approach is accurate to $\lambda/100$ RMS wavefront.

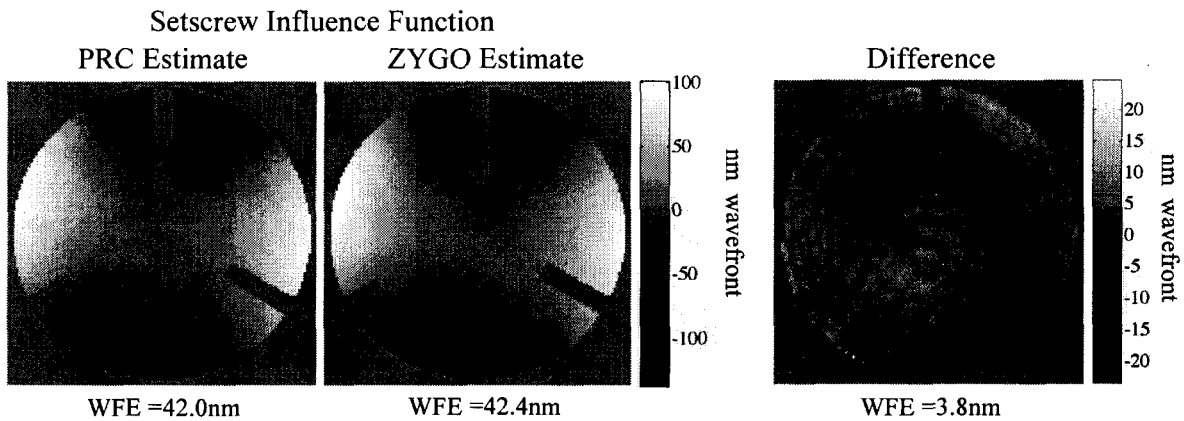


Figure 8: PRC and ZYGO based estimates of the setscrew influence function and their difference

Table 4: Estimation summary of PRC and ZYGO based influence functions.

| Influence Function | RMS WFE (nm) | Net Uncertainty Per Element (nm) |
|--------------------|--------------|----------------------------------|
| PRC | 42.00 | 1.63 |
| ZYGO | 42.36 | 1.57 |
| ZYGO-PRC | 3.81 | 2.26 |

5. CLOSING REMARKS

In this paper we have presented the independent experimental validation of the NGST baseline WFS methodology. Using differential measurements of a test optic in two states of aberration, we demonstrated that MGS based estimates are comparable to the ZYGO interferometer based estimates to a level better than $\lambda/100$ RMS. Furthermore, the small discrepancies between these estimates have a multitude of sources. Along with MGS based WFS error, temporal variations in the test optic mirror figure and alignment repeatability errors account for a portion of the apparent discrepancies.

Regardless, the high level of agreement between the MGS algorithm and the ZYGO validates the MGS approach to be accurate and without significant bias. By coupling this result with previous WFC experiments conducted on the NGST wavefront control testbed, [2], we now have a complete validation of the NGST WFS methodology for both sensing accuracy and spatial bandwidth sensitivity.

ACKNOWLEDGEMENTS

The authors gratefully acknowledge the support of the National Aeronautics and Space Administration.

REFERENCES

1. S. A. Basinger, D. C. Redding, A. E. Lowman, L. A. Burns, K. Liu and D. Cohen, "Performance of wavefront sensing and control algorithms on a segmented telescope testbed," Proc. SPIE, *UV, Optical and IR Space Telescopes and Instruments*, V 4013, pp. 749-756 (2000).
2. C. Bowers, et. al., "Initial test results from the Next Generation Space Telescope wavefront sensing and control testbed," Proc. SPIE, *UV, Optical and IR Space Telescopes and Instruments*, V 4013, pp. 763-773 (2000).
3. A. E. Lowman, D. C. Redding, S. A. Basinger, D. Cohen, J. A. Faust, J. J. Green, C. Ohara, F. Shi, "Phase Retrieval Camera for Testing NGST Optics," Proc. SPIE, *Astronomical Telescopes and Instruments*, Waikoloa, HI, August 22-28 (2002).
4. D. J. Schroeder, *Astronomical Optics*, Academic Press, San Diego, 2000.
5. B. R. Frieden, *Probability, Statistical Optics, and Data Testing*, Springer-Verlag, Berlin, 1991.